LAWRENCE
LIVERMORE
NATIONAL
LABORATORY

LLNL-CONF-424554

Characteristics of Knock in Hydrogen-Oxygen-Argon SI Engine

N. Killingsworth, V. Rapp, D. Flowers, S. Aceves, J-Y. Chen, R. Dibble

February 24, 2010

Western States Section of the Combustion Institute Spring 2010 Meeting
Boulder, CO, United States
March 21, 2010 through March 23, 2010

Disclaimer

2010 Spring Technical Meeting of the Western States Section of the Combustion Institute
Hosted by the University of Colorado at Boulder
March 21-23, 2010
Paper # 10S-68

Characteristics of Knock in Hydrogen-Oxygen-Argon SI Engine

Nick J. Killingsworth[a], Vi H. Rapp[b], Daniel L. Flowers[a], Salvador M. Aceves[a]
J-Y. Chen[b], and Robert Dibble[b]

[a] *Lawrence Livermore National Laboratory, Livermore, CA 94550 USA*
[b] *Department of Mechanical Engineering, University of California-Berkeley, Berkeley, CA 94720 USA*

Abstract
A promising approach for improving the efficiency of internal combustion engines is to employ a working fluid with a high specific heat ratio such as the noble gas argon. Moreover, all harmful emissions are eliminated when the intake charge is composed of oxygen, nonreactive argon, and hydrogen fuel. Previous research demonstrated indicated thermal efficiencies greater than 45% at 5.5 compression ratio in engines operating with hydrogen, oxygen, and argon. However, knock limits spark advance and increasing the efficiency further. Conditions under which knock occurs in such engines differs from typical gasoline fueled engines. In-cylinder temperatures using hydrogen-oxygen-argon are higher due to the high specific heat ratio and pressures are lower because of the low compression ratio. Better understanding of knock under these conditions can lead to operating strategies that inhibit knock and allow operation closer to the knock limit. In this work we compare knock with a hydrogen, oxygen, and argon mixture to that of air-gasoline mixtures in a variable compression ratio cooperative fuels research (CFR) engine. The focus is on stability of knocking phenomena, as well as, amplitude and frequency of the resulting pressure waves.

Keywords: Hydrogen, Internal Combustion Engine, Knock, Noble Gas, Argon

1. Introduction

Reducing emissions of carbon dioxide (CO_2) has become increasingly urgent. Several possible paths exist to achieve CO_2 emissions reductions in the transportation sector: increasing efficiency of petroleum fueled engines, increasing use of alternative fuels, and increasing powertrain electrification with batteries or hydrogen fuel cells. While all of these paths hold some degree of promise, the use of renewable hydrogen (H_2) as a transportation fuel will reduce not only CO_2 emissions, but all carbon based emissions, such as, carbon monoxide (CO) and unburned hydrocarbons. Hydrogen fuel cells are efficient and produce no pollution; however, their high cost is a major barrier limiting their introduction to the mass market. Until fuel cells overcome these barriers, H_2 fueled internal combustion (IC) engines may be a more viable option, since they rely on mature IC engine technology. The only harmful engine-out emissions from H_2 engines are oxides of nitrogen (NO_x), since CO_2 and hydrocarbons from oil consumption are negligible in well-tuned engines. Depending on the operating regime, three-way catalysts, NO_x traps, or ultra lean combustion can efficiently control NO_x emissions.

A more radical approach to NO_x control that may also contribute to increased efficiency consists of replacing nitrogen from the air by an optimized diluent. Noble gases such as helium and argon are promising diluents because of their monatomic structure. These gases are nonreactive and have a high specific heat ratio ($\gamma = 1.67$ compared to $\gamma < 1.4$ for air) because noble gases have only one mode of molecular energy storage: translational motion. Basic engine cycle thermodynamics predicts that the use of a gas with high specific heat ratio leads to high engine efficiency. The indicated engine efficiency

for an ideal Otto cycle can be written as a function of the engine's compression ratio (CR) and the specific heat ratio of in-cylinder gas [1],

$$\eta_i = 1 - \frac{1}{CR^{\gamma-1}}. \quad (1)$$

The relationship between engine efficiency and the specific heat ratio inspired a patent by Laumann et al. [2] in which argon is utilized in an internal combustion (IC) engine. It was proposed that the water from the exhaust would be condensed out and the remaining argon could then be recycled in a closed loop system. This concept was later tested experimentally in a single cylinder spark ignited (SI) Cooperative Fuel Research (CFR) engine by De Boer and Hulet [3]. High efficiency operation was achieved for high concentrations of argon, but knock was a problem at the compression ratios tested, which ranged from 5.5 to 12.

Direct injection compression ignition engines do not suffer from knock and might be a better solution to take advantage of the thermodynamic properties of noble gases. Ikegami et al. [4] experimentally tested this approach and achieved indicated thermal efficiencies close to 50% using compression ratios between 10 and 16. The amount of H_2 they could inject at higher compression ratios was limited due to the injection pressure of their system. High pressure H_2 gas injection is difficult due to the high diffusivity and low lubricity of H_2 gas [5]. Therefore, reliable high-pressure injection of H_2 gas remains an obstacle for the realization of such an engine.

In the near term a low-pressure port injection approach, as opposed to a high pressure direct injection, is more practical. However, as mentioned previously knock can become a problem at compression ratios as low as four. Knock limits spark advance, obstructing the maximum achievable thermal efficiency [6,7]. Understanding knock for this unique mixture of intake gases is important for achieving maximum performance and is the goal of this work.

In this paper we describe the experimental apparatus and tests conducted. Then we present analyze, and discuss the experimental results.

2. Experimental Setup

Experiments were conducted using a single cylinder, port fuel injected, variable compression ratio, ASTM-CFR engine. Engine specifications can be found in Table 1 and a schematic of the experimental configuration is shown in Fig. 1.

In-cylinder pressure was measured using a 6052B Kistler piezoelectric pressure transducer in conjunction with a 5044A Kistler charge amplifier. Intake pressure was measured using a 4045A5 Kistler piezoresistive pressure transducer in conjunction with a 4643 Kistler amplifier module. Sampling of in-cylinder and intake pressures was hardware timed using an optical encoder, and recorded every 0.1 crank angle (CA) degree. An electric motor directly coupled to the engine crankshaft was controlled by an ABB variable speed frequency drive that in turn controlled the engine speed. Mass of H_2 injected was measured using a mass flow sensor (Alicat M Series Mass Flow Meter) and also verified using a Horiba six-gas emissions analyzer. When operating at stoichiometric conditions, $\varphi = 1$, a wide band lambda sensor was primarily used.

Table 1
Engine Specifications

Displacement	Bore	Stroke	Compression Ratio	rpm
0.616 L	82.5 mm	114 mm	4.5-17.5	600-1800

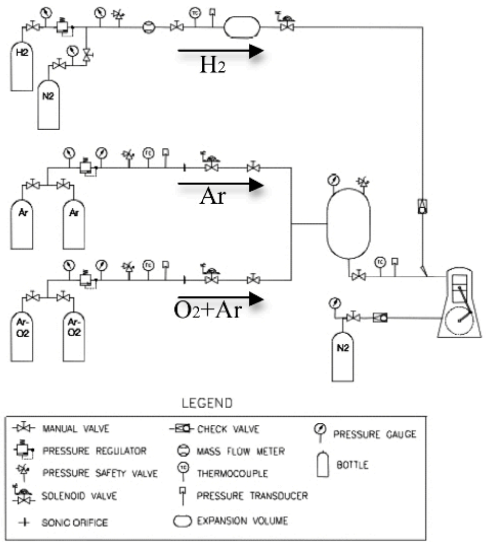

Fig. 1. Schematic diagram of the experimental configuration.

Three sets of high-pressure gas cylinders were used: one containing pure Ar, the second with a mixture of O_2 and Ar, and the third with pure H_2 supplied the engine at specifiable ratios. Pure O_2 could be blended with Ar, for safety reasons, we use O_2 premixed with Ar, which was then blended with Ar. Flow rates of compressed Ar and Ar-O_2 were determined using calibrated sonic orifices. Software controlled electronic pressure regulators set the flow rates by adjusting the gas pressure upstream of the sonic orifices.

A Motec M4 ECU (Engine Control Unit) controlled spark timing, injection timing, and injection pulse width. Initially, when running the engine on H_2-air mixtures, significant problems with backflash (ignition of the fuel before the intake valve closes) occurred. It was found that the backflash occurred because of residual charge in the spark plug wire created from the previous cycle's ignition [8]. Backflash problems ceased after the spark plug wires in our system were modified as described by Kondo et al. [8].

All tests were conducted without throttling the engine at constant intake pressure of 0.98 bar. The engine was pre-heated by burning H_2-air, bringing the coolant temperature to 75°C. This temperature was maintained for the recorded tests using a closed-loop controller. The crankcase was purged with nitrogen (N_2), preventing accidental explosion of any hydrogen that might have blown by the rings.

3. Experimental Results

The CFR engine was fueled with a stoichiometric 91 octane gasoline and air mixture, and stoichiometric H_2-O_2 mixtures diluted with Ar. The spark timing was advanced until knocking occurred.

3.1. Analysis of Pressure Data

The pressure traces, as well as the bandpass filtered pressure traces from the experiments, are shown in figures 2,3 and 4, and Table 2 shows the conditions from the experiments.

Table 2
Experimental conditions

Experiment #	A	B	C
Fuel	91 0ctane gasoline - air	H_2-O_2 84% Ar	H_2-O_2 84% Ar
Compression ratio	7	6	7
RPM	600	900	900
Intake Temperature	50 C	27 C	27 C

Figure 2 shows the pressure traces for experiment A with gasoline at a compression ratio of 7. We can see that knock begins shortly after 30 CAD after TDC. The oscillations can be seen clearly in the lower plot and the peak amplitude hovers around 1.5 bar before decaying.

In Fig. 3 we can see the pressure traces for experiment B with a stoichiometric H_2-O_2 mixture diluted with 84% Ar by volume and a compression of 6. The absolute pressure is slightly lower than that for experiment B due to the lower compression ratio. The amplitude of knock, shown in the bottom of Fig. 3, is also lower and peaks around 0.3 bar. Note that comparing Figs. 2 and 3 the frequency appears to be substantially lower in Fig. 3; this is because the rpm is different, 900 rather than 600, and these figures are presented in the crank angle domain.

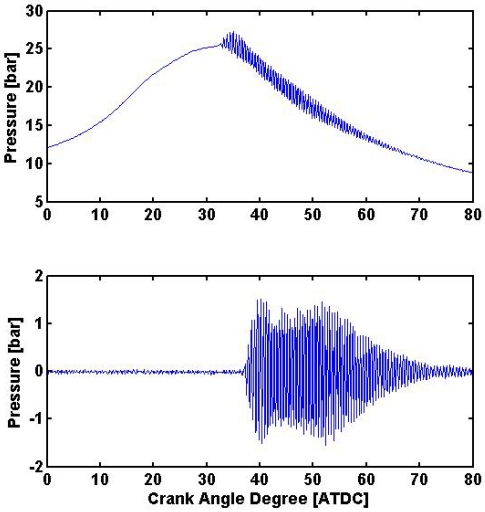

Fig. 2. Absolute (top) and bandpass filtered (bottom) pressure traces with 91 octane gasoline at 600 rpm.

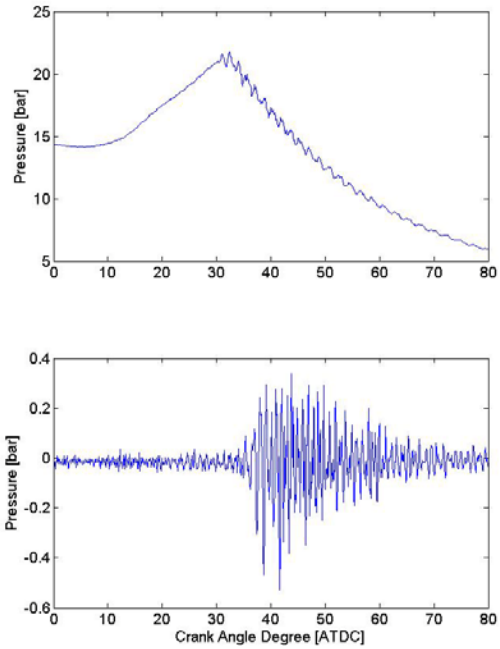

Fig. 3. Absolute (top) and bandpass filtered (bottom) pressure traces with stoichiometric mixture of H_2-O_2 in 84% Ar by volume and compression ratio of 6 at 900 rpm.

Figure 4 shows pressure traces for experiment C with a stoichiometric H_2-O_2 mixture diluted with 84% Ar by volume and a higher compression of 7. The absolute pressure is higher than that of the other two cases due to the higher specific heat ratio of Ar and the higher compression ratio. For this case combustion preceded spark ignition, and occurred due to compression because of the high temperature at TDC and is essentially what occurs in a homogeneous charge compression ignition (HCCI) engine. Because a larger portion of the gas undergoes autoignition the amplitude of the oscillations are much larger than that of the other two cases and is as large as 20 bar.

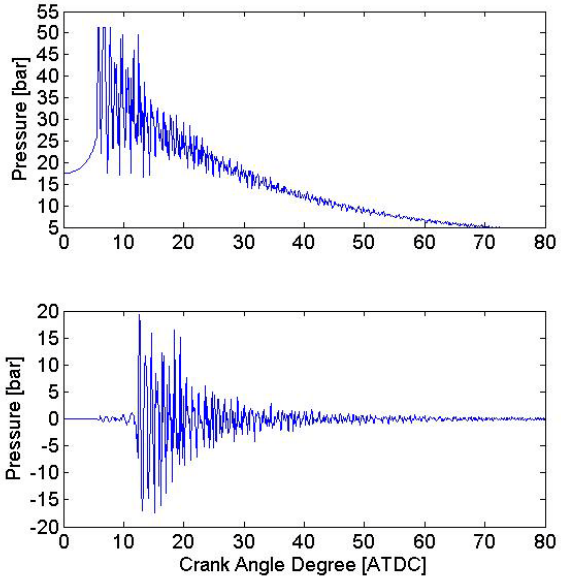

Fig. 4. Absolute (top) and bandpass filtered (bottom) pressure traces with stoichiometric mixture of H_2-O_2 in 84% Ar by volume and compression ratio of 7 at 900 rpm.

To quantify the intensity of the knocking event, we use the maximum of the pressure oscillation (MAPO) [9],

$$MAPO = |p_f|_{max} \qquad (2)$$

where p_f is the filtered in-cylinder pressure. Figure 5 presents the MAPO for 300 cycles for experiment A. We can see from this plot that the MAPO oscillates, but consistently rises above 0.5 bar. For experiment B as shown in Fig. 6 knock does not occur as frequently as for experiment B, but the magnitude reaches above 1 bar, as it does for the gasoline experiments.

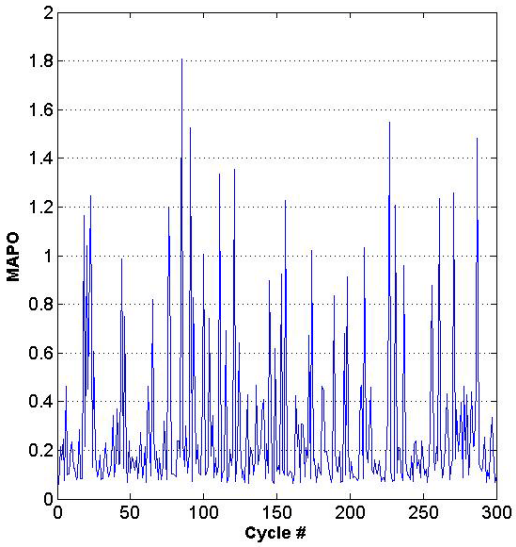

Fig. 5. MAPO for 91 octane gasoline.

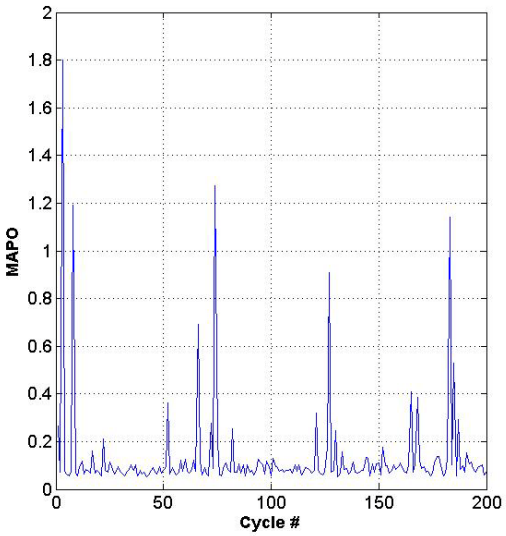

Fig. 6. MAPO for stoichiometric mixture of H_2-O_2 in 84% Ar by volume and compression ratio of 6.

Figure 7 shows that the behavior for experiment C is different than that of experiments A and B. The MAPO is below 0.2 bar until cycle number 134 at which point compression ignition occurs before the spark timing and a large portion of the gas autoignites. Compression ignition occurs every other cycle for the first few cycle and is likely due to the influence of residual gas temperature. The cycles in which compression ignition occurs result in earlier combustion, leading to more heat transfer and lower exhaust temperatures. The increased heat transfer to the walls of the knocking compression

ignition cycles eventually creates conditions capable of sustaining autoigntion every cycle and compression ignition becomes consistent. The fuel is cut off at cycle 145 and the MAPO drops due to the absence of combustion.

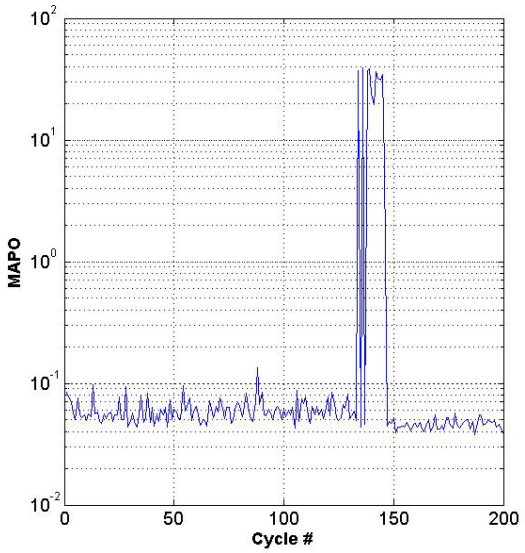

Fig. 7. Log of MAPO for stoichiometric mixture of H_2-O_2 in 84% Ar by volume and compression ratio of 7 and spark timing of 13 CAD BTDC.

3.2. Acoustic Vibration Modes

The first few vibrational modes of the cylinder can be predicted by applying methods developed by Draper [10,11],

$$f_{m,n} = C\frac{\rho_{m,n}}{\pi B} \quad (3)$$

where $\rho_{m,n}$ is the vibrational mode factor and can be found in Table 3 for the first 5 modes, and B is the cylinder bore. The speed of sound is a function of the gas properties

$$C = \sqrt{\gamma RT}. \quad (4)$$

Therefore, the speed of sound increases with an increase in the specific heat ratio of the gas γ, the specific gas constant R, and the gas temperature T. The gas properties, however, vary across the cylinder due to combustion and heat transfer. To calculate the speed of sound for the gasoline experiments, we assume $\gamma = 1.35$ and T = 2200 K, for experiments B and C we assume $\gamma = 1.5$ and a lower temperature of 2000 K due to the higher dilution levels. Although γ is higher for experiments B and C, due to the argon, the effect of the increased molecular weight in equation (4) is much larger and outweighs the effect of gamma. The predicted vibrational frequencies of experiments A, B, and C, using equations 3 and 4, are listed in Table 3. The A, B, and C below the frequencies refer to the experiments listed in Table 2.

Table 3
Acoustic vibration modes and frequencies

m,n	*1,0*	*2,0*	*0,1*	*3,0*	*1,1*
Mode Shape					
$\rho_{m,n}$	1.841	3.054	3.832	4.201	5.332
$f_{m,n}$ kHz (A)	6.7	11.1	13.9	15.2	19.3
$f_{m,n}$ kHz (B,C)	5.6	9.4	11.8	13.0	16.5

3.3. Frequency Analysis of Pressure Traces

The lower plots of figures 2 through 4 show the high frequency content of the pressure traces. A fast Fourier transform (FFT) was performed on each one of these filtered pressure signals and is shown in figures 8 through 10. Figure 8 shows the FFT for one cycle at the conditions of experiment A. The first peak is centered at about 6.3 kHz. We can see from Table 3 that this frequency lies close to the expected first circumferential vibrational mode. It is not clear what the second peak corresponds to, the frequency seems too low to come from a natural vibrational frequency of the chamber, thus it might be due to aliasing of a higher frequency or due to the natural frequency of the cavity preceding the pressure transducer in its adapter. A small peak also exists at 10 kHz, which does correspond to the second circumferential mode.

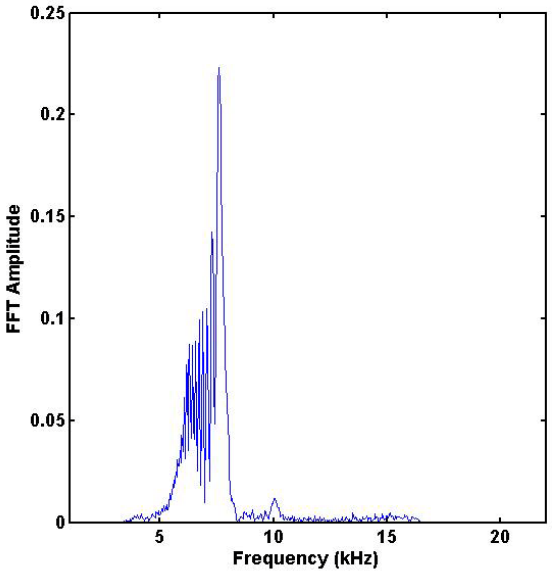

Fig. 8. FFT of in-cylinder pressure trace for 91 octane gasoline.

The FFT for experiment B is presented in Fig. 9. The largest peak occurs at 5.5 kHz, near the predicted first circumferential mode for this mixture. Smaller peaks reside between 9 and 10 kHz, which likely correspond to the second circumferential mode of the cylinder. Another peak lies centered about 16 kHz, which is near the 1,1 mode from Table 3.

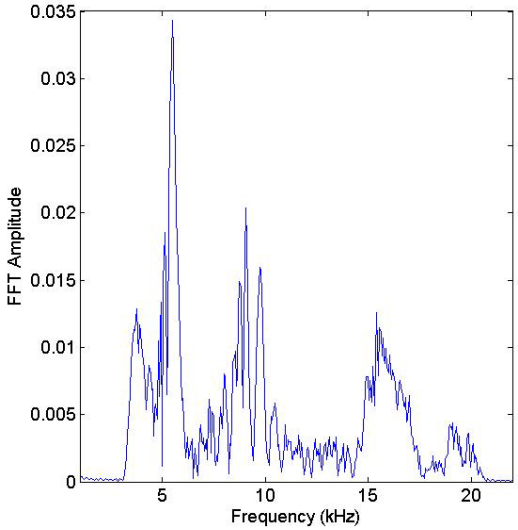

Fig. 9. FFT of in-cylinder pressure trace for stoichiometric mixture of H_2-O_2 in 84% Ar by volume and compression ratio of 6.

The oscillations of the pressure in Fig. 4 are much larger and provide a strong signal; we can see that the amplitude of the FFT in Fig. 10 is much larger than the previous two figures. Again the largest peak is centered at 5.5 kHz, the first circumferential vibrational mode.

4. Conclusions

- The frequencies in the H_2-O_2-Ar mixtures are lower than those found in the gasoline mixture due to changes in the speed of sound from both the lower peak temperature due to decreased mixture energy and increased dilution, as well as the effect of the mixtures molecular weight.
- Combustion was initiated by compression ignition rather than spark ignition while running the engine with a H_2-O_2-Ar mixture and a compression ratio of 7. This HCCI like combustion resulted in large pressure oscillations at the first circumferential mode.

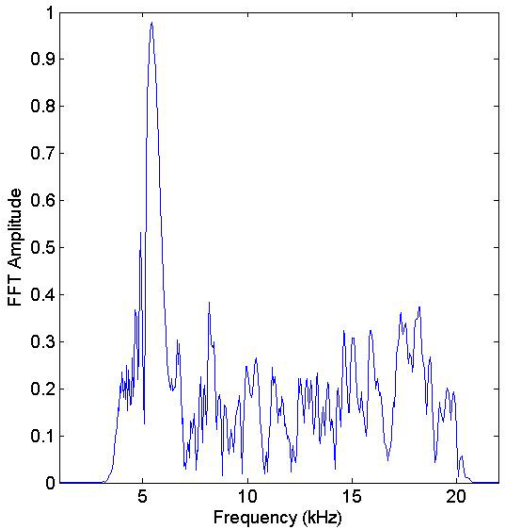

Fig. 10. FFT of in-cylinder pressure trace for stoichiometric mixture of H_2-O_2 in 84% Ar by volume and compression ratio of 7.

Acknowledgments

This work performed under the auspices of the U.S. Department of Energy by Lawrence Livermore National Laboratory under Contract DE-AC52-07NA27344.

References

[1] J.B. Heywood, *Internal combustion engine fundamentals*, New York: McGraw-Hill, 1988.

[2] E.A. Laumann and R.K. Reynolds, "Hydrogen-fueled engine," U.S. Patent 4,112,875, September 1, 1978.

[3] P. deBoer and J. Hulet, "Performance of a hydrogen-oxygen-noble gas engine," *Int. J. Hydrogen Energy*, vol. 5, 1980, pp. 439-452.

[4] M. Ikegami, K. Miwa, and M. Shioji, "A study on hydrogen-fueled compression-ignition engines," *Int. J. Hydrogen Energy*, 1982, pp. 341-353.

[5] A.B. Welch, D. Mumford, S. Munshi, J. Holbery, B. Boyer, M. Younkins, and H. Jung, "Challenges in Developing Hydrogen Direct Injection Technology for Internal Combustion Engines," *SAE Paper, No. 2008-01-2379*, 2008.

[6] J.D. Naber, J.R. Blough, D. Frankowski, M. Goble, and J.E. Szpytman, "Analysis of Combustion Knock Metrics in Spark-Ignition Engines," *SAE Paper No. 2006-01-0400*.

[7] S. Szwaja, K. Bhandary, and J. Naber, "Comparisons of hydrogen and gasoline

combustion knock in a spark ignition engine," *International Journal of Hydrogen Energy*, vol. 32, Dec. 2007, pp. 5076-5087.

[8] T. Kondo, S. Iio, and M. Hiruma, "A Study on the Mechanism of Backfire in External Mixture Formation Hydrogen Engines," *SAE Paper, No. 971704*, 1997.

[9] G. Xiaofeng, R. Stone, C. Hudson, and I. Bradbury, "The Detection and Quantification of Knock in Spark Ignition Engines," *SAE Paper No. 932759*.

[10] C.S. Draper, "Acoustical Analysis of the Pressure Waves Accompanying Detonation in the Internal-Combustion Engine," *The Journal of the Acoustical Society of America*, vol. 10, 1939, p. 259.

[11] M. Brunt, C. Pond, and J. Biundo, "Gasoline Engine Knock Analysis Using Cylinder Pressure Data," *SAE Paper No. 980896*.